# Unvortex Lattice and Topological Defects in Rigidly Rotating Multicomponent Superfluids

Roy Rabaglia,[1] Ryan L. Barnett,[2] and Ari M. Turner[1]
[1] *Department of Physics, Technion, Haifa 32000, Israel*
[2] *Department of Mathematics, Imperial College London, London SW7 2AZ, United Kingdom*
(Dated: April 06, 2024)

By examining the characteristics of a rotating ferromagnetic spinor condensate through the perspective of large spin, we uncover a novel kind of topological point defect in the magnetization texture. These defects are predicted not by the conventional homotopy group analysis but by the Riemann-Hurwitz formula. The spin texture in the system is described by an equal-area mapping from the plane to the sphere of magnetization, forming a lattice of uniformly charged Skyrmions. This lattice carries doubly-quantized (winding number = 2) point defects arranged on the sphere in a tetrahedral configuration. The fluid is found to be rotating rigidly, except at the point defects where the vorticity vanishes. This vorticity structure contrasts with the well-known vortex lattice in scalar rotating superfluids, where vorticity concentrates exclusively within defect points, forming an unconventional "unvortex" lattice. Numerical results are presented, which are in agreement with the aforementioned predictions.

One fundamental characteristic of ordinary (scalar) superfluids is their irrotational flow. In contrast, spinor Bose-Einstein condensates exhibit an intrinsic coupling between the superfluid velocity field $\mathbf{v}(\mathbf{r})$ and the magnetization unit vector field $\hat{\mathbf{n}}(\mathbf{r})$. This coupling is defined by the well-known *Mermin-Ho relation* [1]:

$$(\boldsymbol{\nabla}\times\mathbf{v})_k = \frac{\hbar}{2m} F\varepsilon_{ijk}\hat{\mathbf{n}}\cdot(\partial_i\hat{\mathbf{n}}\times\partial_j\hat{\mathbf{n}}), \qquad (1)$$

where $m$ and $F$ are the mass and spin of each condensed particle, respectively. For a planar ($d = 2$) condensate, this relation holds an intriguing geometrical interpretation: the right-hand side is proportional to the Jacobian of the transformation $\hat{\mathbf{n}}(\mathbf{r}) : \mathbb{R}^2 \to \mathbb{S}^2$ mapping the physical space to the sphere of spin states.

A rich variety of intriguing magnetization textures and flow fields are ubiquitous in spinor condensates [2–20]. One such phenomenon is that the Mermin-Ho relation eliminates the need for vortices of diverging velocity [21–23]. In its ground state, a non-rotating ferromagnetic condensate features uniform magnetization. Upon rotation, maintaining uniform magnetization would lead to an irrotational flow around a quantized vortex lattice, as in ordinary superfluids. However, the Mermin-Ho relation enables energy reduction by adopting non-uniform magnetization, leading to a non-trivial flow field [3, 4, 24–26]. This phenomenon inspires a significant interest in studying the behavior of spinor condensates under rotation.

In this work we provide an analytical approach to study the system using a viewpoint of large spin ($F \gg 1$). Most experimental realizations of spinor condensates have involved spin-1, 2 and 3 atoms [27–32]. Therefore, one might ask 'Why should we care about large spin results?'. First, although spinor condensates of larger spin values have not been realized yet, potential candidates such as spin-6 $^{168}$Er and spin-8 $^{164}$Dy are present [2]. We hope that unveiling the unique properties of larger spin systems will encourage their experimental exploration. Moreover, beyond predicting the characteristics of future condensates, this work aims to establish a framework applicable to explaining properties of smaller spin condensates through perturbative methods. A comparison with numerical simulations for spin values of order 1 shows that the large spin approach explains many of the properties of smaller spin systems effectively. Additionally, a forthcoming publication [33] will describe the system also from the perspective of small spin ($F \ll 1$). Leveraging both limits provides a fairly accurate description for all spin values, even of order 1.

Exploring this system is further motivated by its role as an elegant case study for many interesting concepts. It reveals a novel topological defect in the magnetic texture, relevant to systems involving mappings between topologically inequivalent spaces, such as liquid crystals and topological insulators. These defects impact various properties of the system, such as the flow field, as indicated by the Mermin-Ho relation. Notably, regions of depleted vorticity are formed around the magnetic defects, disrupting a rigid flow for large $F$ condensates. The resulting vortex lattice, shown in Fig. (1), stands as an antithesis to the traditional vortex lattice in superfluids, where all the vorticity concentrates within the defect itself.

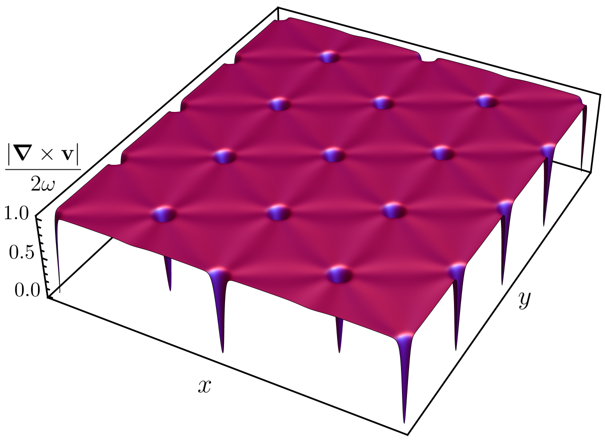


Figure 1. The "unvortex" lattice. Numerical results for the normalized vorticity of an $F = 100$ condensate, displaying a triangular lattice of cores that form around each point defect, where there is a deviation from rigid rotation.

Spinor condensates can exhibit various phases determined by the interatomic interaction parameters [2, 34, 35]. Our focus is on the ferromagnetic phase, which can occur for any $F$ for some range of values of the spin-dependent interactions. Assuming a constant density profile [36], the condensate in this phase can be described solely using the two fields $\mathbf{v}(\mathbf{r})$ and $\hat{\mathbf{n}}(\mathbf{r})$. An alternative description involves angles: the superfluid phase $\theta(\mathbf{r})$, and the magnetic polar and azimuthal angles $\phi(\mathbf{r})$ and $\chi(\mathbf{r})$. Using these angles, the magnetization texture is $\hat{\mathbf{n}} = (\sin\phi\cos\chi, \sin\phi\sin\chi, \cos\phi)$, and the velocity field is

$$\mathbf{v}(\mathbf{r}) = \frac{\hbar}{m}\left[\nabla\theta - F\cos\phi\nabla\chi\right] \tag{2}$$

[37]. This relation is given in the non-rotating frame of reference. Taking the curl yields the Mermin-Ho relation, equivalent to Eq. (1) after rescaling, in terms of $\phi$ and $\chi$:

$$\nabla \times \mathbf{v} = \frac{\hbar}{m}F\sin\phi\nabla\phi \times \nabla\chi. \tag{3}$$

When rotated with an angular velocity of $\boldsymbol{\omega} = \omega\hat{\mathbf{z}}$, the energy functional of the system is

$$E = \frac{\hbar^2\rho}{2m}\int \mathrm{d}^2 r\left[\frac{m^2}{\hbar^2}\left(\mathbf{v} - \boldsymbol{\omega}\times\mathbf{r}\right)^2 + \frac{1}{2}F\left(\nabla\hat{\mathbf{n}}\right)^2\right] \tag{4}$$

[36–38]. We want to identify the important contributions in the large $F$ limit. Although a cursory examination of the energy functional may seem to suggest a dominance of the second (magnetic) term, this overlooks the $F$ dependence of the velocity field, as indicated in Eq. (2). To overcome this issue, we propose employing a rescaling technique.

We rescale the lengths using $\tilde{\mathbf{r}} = F^{-\frac{1}{2}}\mathbf{r}$ to eliminate the dependence of the magnetic term on $F$, and the phase using $\tilde{\theta} = F^{-1}\theta$ to simplify the resulting expression. After both rescalings, the resulting velocity field is expressed as

$$\tilde{\mathbf{v}} = \frac{1}{\sqrt{F}}\mathbf{v} = \frac{\hbar}{m}\left[\tilde{\nabla}\tilde{\theta} - \cos\phi\tilde{\nabla}\chi\right]. \tag{5}$$

As velocity measures the change in position over time, it was also rescaled to account for the rescaling of lengths. This resulting rescaled velocity field is independent of $F$. The energy, which is rescaled by $\tilde{E} = F^{-1}E$ to account for the rescaling of lengths, becomes

$$\tilde{E} = \frac{\hbar^2\rho}{2m}\int \mathrm{d}^2\tilde{r}\left[\frac{m^2}{\hbar^2}F\left(\tilde{\mathbf{v}} - \boldsymbol{\omega}\times\tilde{\mathbf{r}}\right)^2 + \frac{1}{2}\left(\tilde{\nabla}\hat{\mathbf{n}}\right)^2\right]. \tag{6}$$

Contrary to the original energy (4), the rescaled energy functional exhibits a remarkably simple dependence on $F$. Surprisingly, the important term in the large $F$ limit is the kinetic one. Deviations from a state minimizing this term result in a high energetic cost, implying that the condensate rotates rigidly by having a rescaled velocity field of $\tilde{\mathbf{v}} = \boldsymbol{\omega}\times\tilde{\mathbf{r}}$, also indicating $\mathbf{v} = \boldsymbol{\omega}\times\mathbf{r}$. A previous proposal to realize rigidly-rotating superfluids involves the use of spin-orbit coupling [39]. Our study predicts a natural occurrence of this phenomenon in large-$F$ spinor condensates.

The vorticity $\nabla \times \mathbf{v}$ for rigid rotation is a constant, $2\boldsymbol{\omega}$, resulting in a constant right-hand side of the Mermin-Ho relation (3) as well. As mentioned, this expression is proportional to the Jacobian of the mapping $\mathbf{r} \to \hat{\mathbf{n}}(\mathbf{r})$, implying that this mapping must be *area-preserving* (up to a positive scaling factor of $2m\omega/\hbar F$). This Jacobian is also proportional to the Skyrmionic charge density of the system [24, 40, 41], where the Skyrmionic charge $Q$ is the number of times the sphere is covered by the mapping. From this perspective, the area-preserving map describes a system uniformly charged with Skyrmionic charge.

As we shall see shortly, any area-preserving mapping, or more generally, any surjective (covering) mapping from the plane to the sphere, must have defects. These defects can appear in various forms, such as lines or points. Our focus is on point defects, as other types of singularities incur a large amount of energy.

To describe what these point defects are, we use polar coordinates $(r, \alpha)$ on the plane, having the origin placed at a point defect. Additionally, we rotate the sphere such that $\hat{\mathbf{n}}$ points to the north pole at this origin. When this point is encircled, the angle $\chi(r, \alpha)$ must satisfy

$$\chi(r_0, \alpha_0 + 2\pi) = \chi(r_0, \alpha_0) + 2\pi k \tag{7}$$

for every $r_0$ and $\alpha_0$, where $k$ is an integer resembling the winding number. The magnetization texture around such a point forms a $k$-to-1 mapping from the plane to the sphere.

Not every integer $k$ can describe the magnetization texture around a point in the system. Specifically, assuming an area-preserving map, non-positive values ($k \leq 0$) are excluded because the Jacobian of the mapping cannot be strictly positive around them. Additionally, $k = 1$ does not represent the spin texture of a defect but rather a regular 1-to-1 texture, observed around almost all points. Therefore, we define point defects as the $k \geq 2$ points.

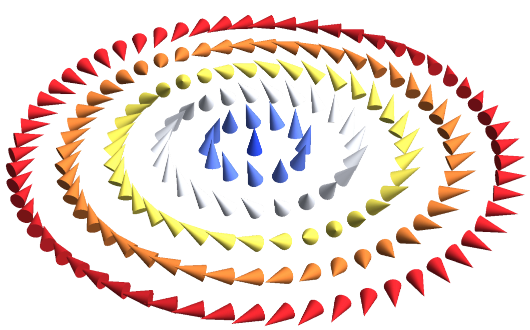

Figure 2. An example of a $k = 2$ spin texture around a defect.

The presence of defects in the mapping $\hat{\mathbf{n}}(\mathbf{r})$ is dictated by the Riemann-Hurwitz formula, a topological theorem that establishes a connection between defects in a mapping and the topological properties of the spaces it connects. Let $P$ and $S$ be two closed Riemann surfaces, and let $\hat{\mathbf{n}} : P \to S$ be a surjective mapping, with no defects other than point defects of the kind described earlier. Suppose that the surface $S$ is covered $Q$ times by the mapping from the entirety of $P$, and suppose that the mapping $\hat{\mathbf{n}}$ has defects at $N$ different points of $P$, where these defects possess the topological numbers $k_1, \ldots, k_N$. Then the Riemann-Hurwitz formula states that

$$2p - 2 = (2s - 2)\, Q + \sum_{i=1}^{N} (k_i - 1)\,, \tag{8}$$

when $p = \text{genus}(P)$ and $s = \text{genus}(S)$ [42–45].

In our case, the mapping $\hat{\mathbf{n}}(\mathbf{r})$ is a mapping from the unit cell $P$ of the spin texture on the plane to the sphere of spin states $S$, and is surjective because any equal-area mapping from the plane to the sphere must be covering. The genus of the unit cell $P$ is $p = 1$ as it is topologically equivalent (homeomorphic) to a torus, and the genus of the sphere $S$ is $s = 0$. Therefore, the Riemann-Hurwitz formula (8) yields

$$2Q = \sum_{i=1}^{N} (k_i - 1)\,. \tag{9}$$

The significant conclusion from this formula is a surprising result: there *must* be stable $k \geq 2$ defects in the system. The formula further emphasizes that a $k = 1$ texture does not describe a defect; $k = 1$ points do not contribute to the Riemann-Hurwitz formula. It is important to note that the defects do not occur just in excited states, but are intrinsic features manifesting even in the ground state of rotating system. This parallels the presence of point defects in the ground state of an ordinary rotating superfluid.

The Riemann-Hurwitz formula provides the number of defects $N$ in each unit cell. Specifically, if all the defects share the same $k$ value, the number of defects in each unit cell is

$$N = \frac{2Q}{k - 1}. \tag{10}$$

By employing both the Riemann-Hurwitz formula and the Mermin-Ho relation, we can also calculate the density of defects. Integrating the Mermin-Ho relation (3) over a unit cell for a rigidly rotating condensate provides us an equation for its area $A$:

$$4\pi Q = \int \sin\phi\, (\boldsymbol{\nabla}\phi \times \boldsymbol{\nabla}\chi) \cdot \hat{z}\, \mathrm{d}^2 r = \frac{2m\omega}{\hbar F} A, \tag{11}$$

which yields

$$A = \frac{2\pi\hbar}{m\omega} F Q. \tag{12}$$

Combining this result with the Riemann-Hurwitz formula (10) yields the density of defects:

$$\frac{N}{A} = \frac{1}{\pi F\,(k - 1)} \frac{m\omega}{\hbar}. \tag{13}$$

Note that $Q$ does not appear in this identity. For a specific condensate rotating at angular velocity $\omega$, the density of the realized defects depends only on their $k$ value. It can be shown that the mapping $\hat{\mathbf{n}}(\mathbf{r})$ is surjective for any value of $F$ (even when it is not area-preserving), making the Riemann-Hurwitz formula applicable also in the general $F$ case. Furthermore, the size of the unit cell (12) remains unchanged regardless of $F$, although the derivation is beyond the scope of this paper. Consequently, the results described here hold true for any $F$ value. Notably, for $F = 1$ and $k = 2$, this formula coincides with the Feynman relation for ordinary vortex lattices [46]. We would like to again underscore the significance of the results derived from the remarkable Riemann-Hurwitz formula: it provides us with a prediction of an entirely new class of topological defects, distinct from the usual kind of topological point defects characterized by the fundamental homotopy group.

As discussed earlier, describing the spin texture for $F = \infty$ involves finding an equal-area mapping from the unit cell to the sphere. Explicitly finding such a mapping is a challenging task, and this paper focuses on explaining the topological structure of the mappings and how considering topological defects aids in understanding it. The objective is to identify the mapping that emerges most simply and naturally (in some sense), given the topological requirements.

The simplest mapping to consider is one that covers the sphere once in total ($Q = 1$). Since the torus and the sphere are topologically inequivalent (having different genus), this cannot be a 1-to-1 mapping (homeomorphism). Consequently, any $Q = 1$ mapping must traverse certain points of the sphere more than once: $M + 1$ times with a positive contribution to $Q$ and $M$ times with a negative contribution to $Q$, where $M$ is an integer greater or equal to 1. However, for a point to contribute negatively to $Q$, the Jacobian of the mapping must be negative at that point, contradicting the requirement of a positive constant Jacobian. Hence, all the suitable mappings must have $Q$ greater than 1.

In order to find a $Q = 2$ mapping, we consider the arrangement of the point defects. Assuming all the defects of the mapping are of the simplest kind, namely $k = 2$, the Riemann-Hurwitz formula (10) implies that there should be $N = 4$ defects in each unit cell. To arrange the images of these four defects on the sphere, we aim for a somewhat symmetrical configuration, considering the rotational symmetry of the problem. A natural arrangement is to embed them on the sphere in the form of a tetrahedron, as if the defects repel each other, akin to charges in the Thomson problem [47].

Now that the four defects are in place, we divide the sphere into four sections using great circles connecting the defect points (see Fig. (3)). These sections are mapped in an equal-area manner onto the faces of a tetrahedron. There are various ways to achieve this, resulting in different equal-area mappings. After the mapping to a tetrahedron, we unfold it to create a planar triangle. Placing two such triangles side by side with reversed orientations forms a parallelogram unit cell, which can be repeated to tile the entire plane. This yields a mapping from the sphere to the plane, which can be inverted to obtain the mapping $\hat{\mathbf{n}}(\mathbf{r})$ from the plane to the sphere. The resulting map is a double covering ($Q = 2$) because each parallelogram unit cell consists of the two triangles, with each triangle covering the sphere once under the mapping $\hat{\mathbf{n}}(\mathbf{r})$. On the plane, the defects are the points around which the corresponding faces of the tetrahedron are repeated twice, resulting in a 2-to-1 texture around them. In the purple-marked unit cell of Fig. (3), there is one defect in the middle of the parallelogram, four halves in the middle of the edges, and a total of one at the vertices of the parallelogram, indeed summing up to a total of four defects.

Numerical minimization of energy (6) using a steepest descent algorithm confirms that the described mapping has the same topological structure as the ground state, even for smaller values of $F$. The ground state lattice is triangular (see Fig. (1)) with tetrahedrally-arranged defects on the sphere. These results are consistent with the prediction of a triangular lattice for pseudospin-1/2 and spin-1 systems[3, 4], and its experimental observation for pseudospin-1/2 [48]. However, the previous analyses have predominantly focused on individual spinor components, unlike our approach, which adopts a geometrical SU (2) and gauge symmetric viewpoint, and reveals the presence and significance of the defects outlined in this paper.

Until now, our focus has centered on understanding the defects through their influence on the magnetic structure. However, due to the Mermin-Ho relation, they also have a crucial effect on the condensate flow. To delve into this aspect, we relax the constraint $\mathbf{v} = \boldsymbol{\omega} \times \mathbf{r}$, allowing us to explore the ground state of a large yet finite $F$ system, utilizing the Euler-Lagrange equations derived from energy (6).

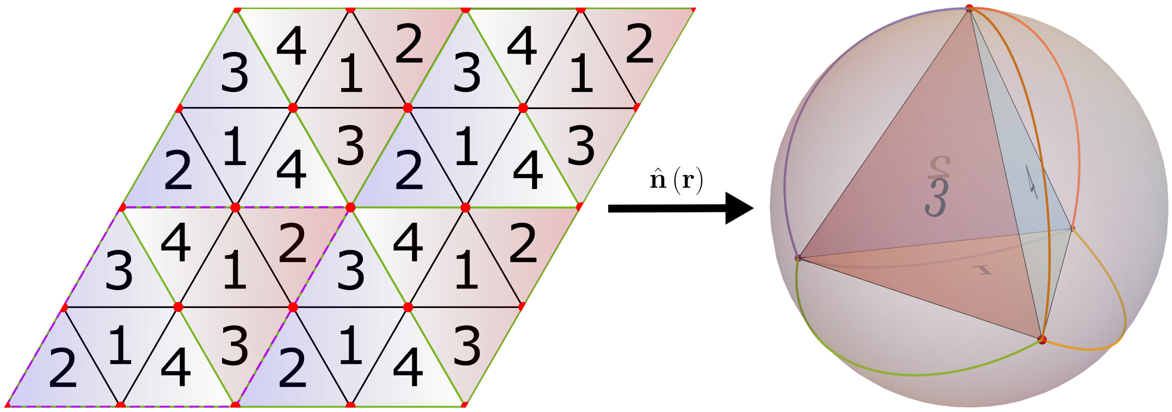


Figure 3. Left: Plane tiled using the tetrahedral mapping. Each unit cell forms a parallelogram, such as the one marked in purple, covers the sphere twice ($Q = 2$), where each of the red and blue triangles covers the sphere once. In each unit cell there are $N = 4$ defect points marked in red. Encircling each of the defects on the plane once corresponds to encircling the corresponding point on the sphere twice, identifying them as $k = 2$ defects. Right: The image on the sphere, including the four defect point (in red) arranged in a tetrahedral shape. The mapping $\hat{\mathbf{n}}(\mathbf{r})$ is generated by "shrinking" (and rescaling) the sphere to the tetrahedron in an equal-area manner, opening the tetrahedron to a planar triangle, and inverting the resulting map. The great circles connecting the defects are mapped to the edges of the tetrahedron, enclosing the regions that are mapped to each of the tetrahedron faces.

It can be shown that for an area-preserving mapping the second derivatives of $\hat{\mathbf{n}}$ with respect to $\mathbf{r}$ diverge at the defects, causing the torque $\delta E/\delta\phi$ acting on $\hat{\mathbf{n}}$ to diverge. Consequently, such a mapping is valid only for infinite $F$, and should be replaced with another solution near the defects for any finite $F$. To address this, we study the cores of the defects, defined as the regions where the area-preserving approximation breaks down significantly, and characterized by a notable deviation of the vorticity from the rigid rotation value $2\boldsymbol{\omega}$, as can be seen in Fig. (1). This definition differs from the typical defect core definition, such as in scalar superfluid vortices, which is based on a significant reduction in density. In this sense, the defects we describe are coreless.

In the limit of large $F$, the area on the plane occupied by each of the cores is independent of $F$. According to the Mermin-Ho relation, the area corresponding to the image of the core on the sphere is proportional to $F^{-1}$, hence its angular size scales as $\phi \sim F^{-\frac{1}{2}}$. For large $F$, this section is small, therefore appearing flat, which allows the Euler-Lagrange equations in this region to be simplified by neglecting the curvature of the sphere. By rotating $\hat{\mathbf{n}}$ at the defect to the north pole, and assuming a rotationally invariant structure in the vicinity of the defect, we may take $\chi = k\alpha$ in order to describe a $k$-defect. The approximated Euler-Lagrange equation for $\phi$ is then:

$$x\frac{\partial}{\partial x}\left(x\frac{\partial u}{\partial x}\right) = \left(k^2 - 2kx^2\right)u + k^2u^3, \tag{14}$$

where $u = \sqrt{F}\phi$, and $\mathbf{x} = \sqrt{m\omega/\hbar}\mathbf{r}$ is a non-dimensional form of the coordinates. Since this equation is independent of the parameters, the typical scales for $u$ and $x$ are of order 1, justifying the scales mentioned earlier. In the original variables, the core area on the plane is of order $m\omega/\hbar$ and therefore for large $F$, the unit cell size, given by Eq. (12), is much larger than the core size. Hence, the cores are far apart, validating the analysis of each core separately. While for the area-preserving case $u \propto x$ near the defect, the solution of Eq. (14) yields $u \propto x^k$. This corrects the aforementioned singularities in the second derivatives of $\hat{\mathbf{n}}$, resulting in an infinitely differentiable magnetization texture.

After rescaling, the Mermin-Ho relation around the defect becomes

$$\boldsymbol{\nabla} \times \mathbf{v} = \omega\frac{k}{2x}\frac{\partial u^2}{\partial x}\hat{z}. \tag{15}$$

Numerical solution of Eq. (14) for $u(x)$ yields the vorticity inside the core, shown in Fig. (4). The vorticity grows from 0 to $2\omega$ on the scale of $x = 1$, consistent with the expected core size. Comparison with one of the defects in the numerical results described above shows convergence towards the predicted curve as $F$ increases. A notable difference between the theoretical curve and the finite $F$ solutions is that the vorticity exceeds $2\omega$ for large $x$. This discrepancy, also visible in Fig. (1), results from finite $F$ corrections outside of the core, and will be addressed in a subsequent paper [33].

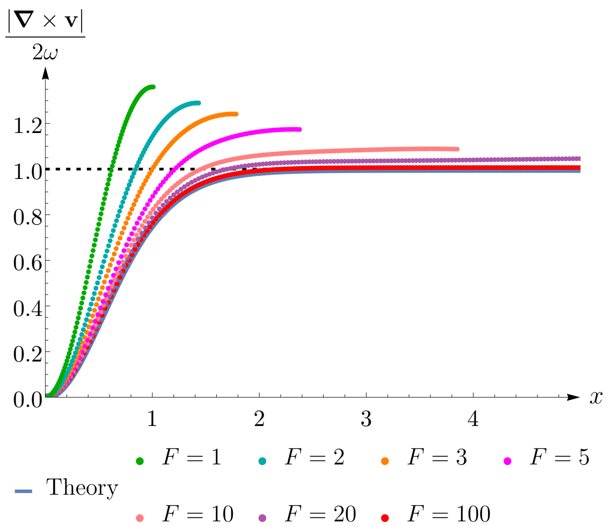


Figure 4. Line: normalized vorticity around a $k = 2$ defect, calculated from Eq. (15) using the numerical solution of (14). Points: numerical gradient descent simulation results for the normalized angle-averaged vorticity around a defect for various values of $F$.

The contrast between the defects of the velocity field in our system and conventional superfluid vortices is evident. In our system, vorticity increases gradually from zero at the defect point to $2\boldsymbol{\omega}$ as we move away, whereas in regular superfluid vortices, all the vorticity is concentrated within the defect itself. This analysis, supported by independent numerical results, shows that the positions of the "unvortices" align precisely with the locations of the magnetic texture defects. This alignment establishes a connection between the defects of the fields $\mathbf{v}(\mathbf{r})$ and $\hat{\mathbf{n}}(\mathbf{r})$, despite their fundamentally different nature.

We would like to thank Hillel Aharoni for suggesting the term "unvortex", and Sandro Stringari for promoting initial interest in problem of rigidly rotating superfluids. RB acknowledges support from the European Union's Seventh Framework Programme under Grant No. PCIG-GA2013-631002. AMT acknowledges support from the Israeli Science Foundation (ISF) Grant No. 1939/18. RB and AMT thank the hospitality of the Aspen Center for Physics under Grant No. PHYS-1066293.

## REFERENCES

[1] Mermin, N. D., and Tin-Lun Ho, *Circulation and angular momentum in the a phase of superfluid Helium-3*, Physical Review Letters 36.11: 594 (1976).

[2] Kawaguchi, Yuki, and Masahito Ueda, *Spinor Bose–Einstein condensates*, Physics Reports 520.5: 253-381 (2012).

[3] Mueller, Erich J., and Tin-Lun Ho, *Two-component Bose-Einstein condensates with a large number of vortices*, Physical review letters 88.18: 180403 (2002).

[4] J. W. Reijnders, F. J. M. van Lankvelt, and K. Schoutens, *Rotating spin-1 bosons in the lowest Landau level*, Physical Review A 69.2: 023612 (2004).

[5] Yi, S., and H. Pu, *Spontaneous spin textures in dipolar spinor condensates*, Physical review letters 97.2: 020401 (2006).

[6] Kawaguchi, Y., Saito, H. and Ueda, Masahito, *Einstein–de Haas effect in dipolar Bose-Einstein condensates*, Physical review letters 96.8: 080405 (2006).

[7] Zhang, Wenxian, Ö. E. Müstecaplıoğlu, and L. You, *Solitons in a trapped spin-1 atomic condensate*, Physical Review A 75.4: 043601 (2007).

[8] P. Simula, T., AM Huhtamäki, J., Takahashi, M., Mizushima, T. and Machida, K., *Rotating dipolar spin-1 Bose–Einstein condensates*, Journal of the Physical Society of Japan 80.1: 013001 (2010).

[9] Cherng, R. W., and E. Demler, *Neutral skyrmion configurations in the low-energy effective theory of spinor-condensate ferromagnets*, Physical Review A 83.5: 053614 (2011).

[10] Song, S. W., Wen, L., Liu, C. F., Gou, S. C., and Liu, W. M., *Ground states, solitons and spin textures in spin-1 Bose-Einstein condensates*, Frontiers of Physics 8: 302-318 (2013).

[11] Huang, Chao-Chun, and S-K. Yip, *Dynamics and complex structure of two-dimensional skyrmions in antiferromagnetic spin-1 Bose-Einstein condensates*, Physical Review A 88.1: 013628 (2013).

[12] Kaneda, Tomoya, Saito, *Dynamics of a vortex dipole across a magnetic phase boundary in a spinor Bose-Einstein condensate*, Physical Review A 90.5: 053632 (2014).

[13] Seo, S. W., Kang, S., Kwon, W. J., and Shin, Y. I., *Half-quantum vortices in an antiferromagnetic spinor Bose-Einstein condensate*, Physical Review Letters 115.1: 015301 (2015).

[14] Mawson, T., Ruben, G., and Simula, T., *Route to non-Abelian quantum turbulence in spinor Bose-Einstein condensates*, Physical Review A 91.6: 063630 (2015).

[15] Borgh, M. O., Nitta, M., and Ruostekoski, J., *Stable core symmetries and confined textures for a vortex*

*line in a spinor bose-einstein condensate*, Physical review letters 116.8: 085301 (2016).

[16] Li, Y., Luo, Z., Liu, Y., Chen, Z., Huang, C., Fu, S., Tan, H. and Malomed, B. A., *Two-dimensional solitons and quantum droplets supported by competing self-and cross-interactions in spin-orbit-coupled condensates*, New Journal of Physics 19.11: 113043 (2017).

[17] Sonin, E. B., *Spin and mass superfluidity in a ferromagnetic spin-1 Bose-Einstein condensate*, Physical Review B 97.22: 224517 (2018).

[18] Zamora-Zamora, R., and V. Romero-Rochín, *Skyrmions with arbitrary topological charges in spinor Bose–Einstein condensates*, Journal of Physics B: Atomic, Molecular and Optical Physics 51.4: 045301 (2018).

[19] Luo, H. B., Li, L., and Liu, W. M., *Three-Dimensional Skyrmions with Arbitrary topological number in a Ferromagnetic Spin-1 Bose-Einstein condensate*, Scientific Reports 9.1: 18804 (2019).

[20] Mithun, T., Carretero-González, R., Charalampidis, E. G., Hall, D. S., and Kevrekidis, P. G., *Existence, stability, and dynamics of monopole and Alice ring solutions in antiferromagnetic spinor condensates*, Physical Review A 105.5: 053303 (2022).

[21] Martikainen, J-P., A. Collin, and K-A. Suominen, *Coreless vortex ground state of the rotating spinor condensate*, Physical Review A 66.5: 053604 (2002).

[22] Leanhardt, A. E., Shin, Y. I., Kielpinski, D., Pritchard, D. E., and Ketterle, W. , *Coreless vortex formation in a spinor Bose-Einstein condensate*, Physical review letters 90.14: 140403 (2003).

[23] Mizushima, T., Kobayashi, N., and Machida, K., *Coreless and singular vortex lattices in rotating spinor Bose-Einstein condensates*, Physical Review A 70.4: 043613 (2004).

[24] Kasamatsu, K., Tsubota, M., and Ueda, M., *Vortices in multicomponent Bose–Einstein condensates*, International Journal of Modern Physics B 19.11: 1835-1904 (2005).

[25] Lovegrove, J., Borgh, M. O., and Ruostekoski, J., *Energetically stable singular vortex cores in an atomic spin-1 Bose-Einstein condensate*, Physical Review A 86.1: 013613 (2012).

[26] Xu, X. Q., and Han, J. H., *Spin-orbit coupled Bose-Einstein condensate under rotation*, Physical Review Letters 107.20: 200401 (2011).

[27] M.-S. Chang, C. D. Hamley, M. D. Barrett, J. A. Sauer, K. M. Fortier, W. Zhang, L. You, and M. S. Chapman, *Observation of spinor dynamics in optically trapped* $^{87}$Rb *Bose-Einstein condensates*, Physical Review Letters 92.14: 140403 (2004).

[28] Black, A. T., Gomez, E., Turner, L. D., Jung, S., and Lett, P. D., *Spinor dynamics in an antiferromagnetic spin-*1 *condensate*, Physical Review Letters 99.7: 070403 (2007).

[29] Kuwamoto, T., Araki, K., Eno, T., and Hirano, T., *Magnetic field dependence of the dynamics of* $^{87}$Rb *spin-*2 *Bose-Einstein condensates*, Physical Review A 69.6: 063604 (2004).

[30] H. Schmaljohann, M. Erhard, J. Kronjäger, M. Kottke, S. van Staa, L. Cacciapuoti, J. J. Arlt, K. Bongs, and K. Sengstock, *Dynamics of $F = 2$ spinor Bose-Einstein condensates*, Physical Review Letters 92.4: 040402 (2004).

[31] Pasquiou, B., Maréchal, E., Bismut, G., Pedri, P., Vernac, L., Gorceix, O., and Laburthe-Tolra, B., *Spontaneous demagnetization of a dipolar spinor Bose gas in an ultralow magnetic field*, Physical Review Letters 106.25: 255303 (2011).

[32] Huh, S., Kim, K., Kwon, K., and Choi, J. Y., *Observation of a strongly ferromagnetic spinor Bose-Einstein condensate*, Physical Review Research 2.3: 033471 (2020).

[33] Rabaglia, R., Barnett, R. L., Turner. A. M., in progress.

[34] Lamacraft, Austen, *Low-energy dynamics of spinor condensates*, Physical Review B 81.18: 184526 (2010).

[35] Borgh, M. O., and Ruostekoski, J., *Topological interface physics of defects and textures in spinor Bose-Einstein condensates*, Physical Review A 87.3: 033617 (2013).

[36] Lamacraft, Austen, *Long-wavelength spin dynamics of ferromagnetic condensates*, Physical Review A 77.6: 063622 (2008).

[37] Lamacraft, Austen, *Persistent currents in ferromagnetic condensates*, Physical Review B 95.22: 224512 (2017).

[38] The contributions of centrifugal forces and trap potential may disrupt the assumption of constant density profile. However, except near the edges of the condensate, these effects can be neglected due to strong interatomic interactions, rendering them absent from the energy functional.

[39] Stringari, Sandro, *Diffused vorticity and moment of inertia of a spin-orbit coupled Bose-Einstein condensate*, Physical Review Letters 118.14: 145302 (2017).

[40] Rajaraman, Ramamurti, *Solitons and instantons*, Elsevier Science Publishers (1982).

[41] Han, Jung Hoon, *Skyrmions in condensed matter*, Vol. 278. Berlin: Springer (2017).

[42] Riemann, Bernhard, *Gesammelte mathematische Werke und wissenschaftlicher Nachlass*, BG Teubner (1876).

[43] Hurwitz, Adolf, *Ueber Riemann'sche Flächen mit gegebenen Verzweigungspunkte*, Mathematische Werke 1 , Birkhäuser pp. 321–383 (1932).

[44] Beardon, Alan F., *Iteration of rational functions: Complex analytic dynamical systems,* Vol. 132. Springer Science & Business Media (2000).

[45] Donaldson, Simon, *Riemann surfaces*, Oxford University Press (2011).

[46] Feynman, Richard P., *Chapter II: application of quantum mechanics to liquid helium*, Progress in low temperature physics. Vol. 1. Elsevier. 17-53 (1955).

[47] Thomson, J. J., *XXIV. On the structure of the atom: an investigation of the stability and periods of oscil-*

*lation of a number of corpuscles arranged at equal intervals around the circumference of a circle; with application of the results to the theory of atomic structure*, The London, Edinburgh, and Dublin Philosophical Magazine and Journal of Science, 7(39), 237-265 (1904)..

[48] Schweikhard, Volker, et al., *Vortex-lattice dynamics in rotating spinor Bose-Einstein condensates*, Physical review letters 93.21: 210403 (2004).